Journal of Power Sources 195 (2010) 7225–7229

Contents lists available at ScienceDirect

Journal of Power Sources

journal homepage: www.elsevier.com/locate/jpowsour

Short communication

Effect of Gd and Yb co-doping on structure and electrical conductivity of the $Sm_2Zr_2O_7$ pyrochlore

Zhan-Guo Liu [a], Jia-Hu Ouyang [a,*], Ke-Ning Sun [b], Xiao-Liang Xia [a]

[a] Institute for Advanced Ceramics, Department of Materials Science, Harbin Institute of Technology, PO Box 433, No. 92 West Da-Zhi Street, Harbin, Heilongjiang 150001, China
[b] Academy of Fundamental and Interdisciplinary Sciences, Harbin Institute of Technology, No. 92 West Da-Zhi Street, Harbin 150001, China

ARTICLE INFO

Article history:
Received 4 April 2010
Received in revised form 31 May 2010
Accepted 31 May 2010
Available online 8 June 2010

Keywords:
$SmYb_{1-x}Gd_xZr_2O_7$
Structure
Impedance spectroscopy
Electrical conductivity

ABSTRACT

$SmYb_{1-x}Gd_xZr_2O_7$ ($0 \le x \le 1.0$) ceramics were pressureless-sintered at 1973 K for 10 h in air. The relative density, structure and electrical conductivity of $SmYb_{1-x}Gd_xZr_2O_7$ ceramics were investigated by the Archimedes method, X-ray diffraction, scanning electron microscopy and impedance spectroscopy measurements. $SmYb_{1-x}Gd_xZr_2O_7$ ($0 \le x \le 0.5$) ceramics exhibit a defect fluorite-type structure, while $SmYb_{1-x}Gd_xZr_2O_7$ ($0.7 \le x \le 1.0$) ceramics have a pyrochlore-type structure. The measured values of the electrical conductivities obey the Arrhenius relation. The grain conductivity of each composition in $SmYb_{1-x}Gd_xZr_2O_7$ ceramics increases with increasing temperature from 723 to 1173 K. The grain conductivity of $SmYb_{1-x}Gd_xZr_2O_7$ ceramics gradually increases with increasing gadolinium content at identical temperature levels. An increase of about one order of magnitude in grain conductivity is found at all temperature levels when the gadolinium content increases from 0.5 to 0.7. $SmYb_{1-x}Gd_xZr_2O_7$ ceramics are oxide-ion conductors in the oxygen partial pressure range of 1.0×10^{-4} to 1.0 atm at all test temperature levels. The highest grain conductivity value obtained in this work is 2.69×10^{-2} S cm^{-1} at 1173 K for $SmGdZr_2O_7$ ceramic.

1. Introduction

In recent years, $A_2B_2O_7$-type ternary oxides (A = lanthanide, B = Zr, Hf, Ce, Ti, etc.) have attracted great interests due to their important physical and chemical properties [1–6]. These complex oxides exhibit a pyrochlore-type structure or a defect fluorite-type structure, which is mainly governed by the radii of A- and B-site cations [7]. Especially, they are potential solid electrolytes due to their excellent electrical properties for intermediate-temperature solid oxide fuel cells applications. It is well known that electrical conductivities of oxide electrolytes are affected by various factors such as oxygen vacancy concentration, crystal structure, ionic radius of doping elements, etc. [8–10]. The electrical conductivity of $Sm_2Zr_2O_7$ pyrochlore was comparable to those of other good oxide-ion conductors in low-temperature regions, and was approximately constant in an oxygen partial pressure range of 1.0×10^{-20} to 1 atm below 1087 K [11]. Lowering the operating temperature of solid oxide fuel cells has attracted great interest worldwide. Enormous amounts of efforts were made to further improve the electrical conductivity of oxide electrolytes [12–14]. Recently, new $A_2B_2O_7$-type oxides with various cation radius ratios of $r(A^{3+})/r(B^{4+})$ are of considerable scientific interest [15–20]. A significant increase in electrical conductivity was found by suitable substitution of isovalent rare earth cations like Nd or Sm at the Gd site in $Gd_2Zr_2O_7$ ceramic [15,16]. The electrical conductivities of $(Gd_{1-x}La_x)Zr_2O_7$ ($0 \le x \le 1.0$) ceramics prepared by mechanically milling stoichiometric mixtures of the corresponding oxides were almost La-content independent from 773 to 1023 K [17,18]. For $(Sm_{1-x}Y_x)_2Zr_2O_7$ ($0 \le x \le 0.5$) and $(Sm_{1-x}Yb_x)_2Zr_2O_7$ ($0 \le x \le 1.0$) ceramics, the electrical conductivities of pyrochlore-type materials were obviously higher than those of defect fluorite-type materials in the temperature range of 723–1073 K [19,20].

In the present work, $SmYb_{1-x}Gd_xZr_2O_7$ ($0 \le x \le 1.0$) ceramic powders were firstly synthesized by a chemical-coprecipitation and calcination technique, and were then pressureless-sintered at 1973 K for 10 h in air. The objective of this work is to study the effect of gadolinium and ytterbium co-doping on structure and electrical conductivity of the $Sm_2Zr_2O_7$ pyrochlore.

2. Experimental procedure

In the present study, ceramic powders of Gd and Yb co-doped $Sm_2Zr_2O_7$, $SmYb_{1-x}Gd_xZr_2O_7$ (x = 0, 0.1, 0.3, 0.5, 0.7, 0.9, and 1.0), were synthesized by a chemical-coprecipitation and calcination technique. Starting materials of rare earth oxides (Sm_2O_3, Gd_2O_3 and Yb_2O_3, Rare-Chem Hi-Tech Co., Ltd., Huizhou, China; purity

* Corresponding author. Tel.: +86 451 86414291; fax: +86 451 86414291.
E-mail address: ouyangjh@hit.edu.cn (J.-H. Ouyang).

0378-7753/$ – see front matter © 2010 Elsevier B.V. All rights reserved.
doi:10.1016/j.jpowsour.2010.05.064

≥99.99%) and $ZrOCl_2{\cdot}8H_2O$ (Zibo Huantuo Chemical Co., Ltd., China; Analytical) were used without further purification. Rare earth oxides were heat-treated at 1173 K for 2 h in air before further use. For each composition, appropriate quantity of rare earth oxides was dissolved in dilute nitric acid, while $ZrOCl_2{\cdot}8H_2O$ was dissolved in distilled water. These solutions were mixed, stirred, filtered, and slowly added under stirring to excessive dilute ammonium hydrate solution to obtain gel-like precipitates. These gels were washed, dried and then calcined at 1073 K for 5 h in air. The obtained ceramic powders were compacted by cold isostatic pressing at 280 MPa for 5 min, and the compacts were pressureless-sintered at 1973 K for 10 h in air.

The phase structures of sintered ceramics were identified by an X-ray diffractometer (Rigaku D/Max 2200VPC, Japan) with Cu Kα radiation at a scan rate of 4° min^{-1}. The diffraction peaks of $(3\,1\,1)_F/(6\,2\,2)_{Py}$ were recorded in a step-scan mode with a step-width of 0.02° and a step-time of 3 s. In order to evaluate the lattice constants, silicon powder was used as the external standard. The theoretical density of each composition was calculated using lattice parameters acquired from XRD results and the molecular weight in an elementary cell. The bulk density of each specimen was measured by the Archimedes method with an immersion medium of deionized water. The morphology of $SmYb_{1-x}Gd_xZr_2O_7$ ceramics was observed by scanning electron microscopy (Hitachi S-4700, Japan) on polished and thermally etched (1873 K, 1 h) surfaces. The impedance spectra of $SmYb_{1-x}Gd_xZr_2O_7$ ceramics were measured by an impedance/gain-phase analyzer (Solatron™ SI 1260, UK) over a frequency range of 20 Hz to 2 MHz. The dimensions of each specimen were about 8 mm in diameter and 1 mm in thickness. The measurements were carried out at temperatures between 723 and 1173 K in air using platinum wires and platinum paste as contacts. Oxygen partial pressure $p(O_2)$ dependence of impedance spectra of $SmYb_{1-x}Gd_xZr_2O_7$ ceramics was also measured in the $p(O_2)$ range of 1.0×10^{-4} to 1.0 atm.

3. Results and discussion

Fig. 1(a) reveals the room temperature X-ray diffraction patterns of $SmYb_{1-x}Gd_xZr_2O_7$ ceramics sintered at 1973 K for 10 h in air. It can be seen that $SmYb_{1-x}Gd_xZr_2O_7$ ceramics have a single phase structure. From Fig. 1(a), $SmYb_{1-x}Gd_xZr_2O_7$ ($0 \le x \le 0.5$) ceramics exhibit a defect fluorite-type structure. However, the situation is different when the gadolinium content is more than 0.5. With further incorporation of larger Gd^{3+} cations, $SmYb_{1-x}Gd_xZr_2O_7$ ($0.7 \le x \le 1.0$) ceramics transform into a pyrochlore-type structure, which is characterized by the presence of typical superstructure peaks at 2θ values of about 14° (1 1 1), 28° (3 1 1), 37° (3 3 1), 45° (5 1 1) and 51° (5 3 1) using Cu Kα radiation [4,21,22].

In the $Ln_2Zr_2O_7$ system, the phase structure is mainly governed by the ionic radius ratio of $r(Ln^{3+})/r(Zr^{4+})$. The stability of pyrochlore-type structure in zirconates is limited to the range of $1.46 \le r(Ln^{3+})/r(Zr^{4+}) \le 1.78$ at an atmospheric pressure [7]. Below 1.46, the array of unoccupied anion sites disorders, to produce a defect fluorite structure. Above 1.78, there is a transition to a monoclinic phase with a $La_2Ti_2O_7$-type structure. The ionic radius of Zr^{4+} is 0.072 nm in the sixfold coordination; however, the ionic radii of Sm^{3+}, Gd^{3+} and Yb^{3+} are 0.1079, 0.1053 and 0.0985 nm in eightfold coordination, respectively [23]. The average ionic radius, $r(Ln_{av.}{}^{3+})$, of the *Ln*-sites in the $SmYb_{1-x}Gd_xZr_2O_7$ ceramics is estimated from the ionic radii of the component ions and the chemical composition using the following equation [24]:

$$r(Ln_{av.}^{3+}) = \frac{r(Sm^{3+}) + xr(Gd^{3+}) + (1-x)r(Yb^{3+})}{2} \quad (1)$$

The values of $r(Ln^{3+})/r(Zr^{4+})$ are clearly lower than 1.46 for $SmYb_{1-x}Gd_xZr_2O_7$ ($0 \le x \le 0.5$) ceramics, respectively, and there-

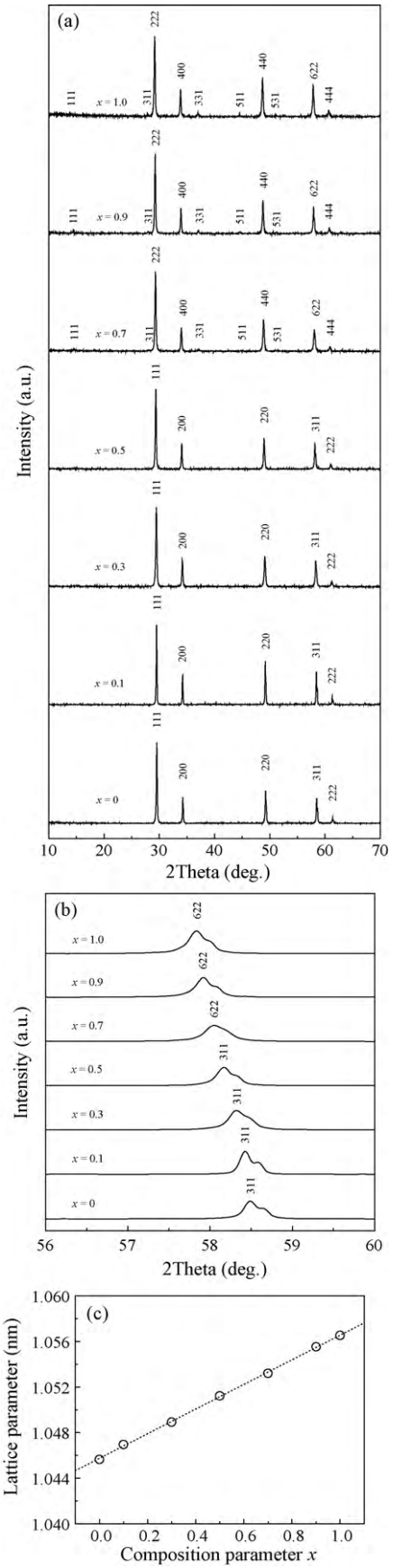

Fig. 1. XRD patterns and derived lattice parameters of $SmYb_{1-x}Gd_xZr_2O_7$ ceramics: (a) in a 2θ range of 10–70°; (b) a single $(3\,1\,1)_F/(6\,2\,2)_{Py}$ peak; (c) lattice parameters derived from (b).

Table 1
Relative densities of $SmYb_{1-x}Gd_xZr_2O_7$ ceramics sintered at 1973 K for 10 h in air.

Ceramic materials	Relative density (%)
$SmYbZr_2O_7$	96.6
$SmYb_{0.9}Gd_{0.1}Zr_2O_7$	96.2
$SmYb_{0.7}Gd_{0.3}Zr_2O_7$	96.0
$SmYb_{0.5}Gd_{0.5}Zr_2O_7$	98.0
$SmYb_{0.3}Gd_{0.7}Zr_2O_7$	97.5
$SmYb_{0.1}Gd_{0.9}Zr_2O_7$	97.2
$SmGdZr_2O_7$	97.7

fore $SmYb_{1-x}Gd_xZr_2O_7$ $(0 \le x \le 0.5)$ ceramics exhibit a defect fluorite-type structure. As for the other zirconate ceramics in this work, $SmYb_{1-x}Gd_xZr_2O_7$ $(0.7 \le x \le 1.0)$, the values of $r(Ln^{3+})/r(Zr^{4+})$ are higher than 1.46, and therefore $SmYb_{1-x}Gd_xZr_2O_7$ $(0.7 \le x \le 1.0)$ ceramics exhibit a pyrochlore-type structure.

Fig. 1(b) shows the X-ray diffraction patterns of $SmYb_{1-x}Gd_xZr_2O_7$ ceramics in the 2θ range of 56–60°. The $(3\,1\,1)_F/(6\,2\,2)_{Py}$ peaks gradually shift to the low angle side for $SmYb_{1-x}Gd_xZr_2O_7$ ceramics with increasing gadolinium content. The lattice parameters calculated from these peaks in relation to the pyrochlore-type unit cell are depicted in Fig. 1(c). An approximately linear increase of the lattice parameter is observed for $SmYb_{1-x}Gd_xZr_2O_7$ ceramics with increasing gadolinium content, which is in a good agreement with the Vegard's rule. The relative densities of $SmYb_{1-x}Gd_xZr_2O_7$ ceramics sintered at 1973 K for 10 h in air vary between 96 and 98%, as shown in Table 1. The results obtained from SEM observations indicate that $SmYb_{1-x}Gd_xZr_2O_7$ ceramics are very dense. The morphology of grains is similar for $SmYb_{1-x}Gd_xZr_2O_7$ ceramics sintered at 1973 K for 10 h in air. The typical thermally etched surface morphology of $SmYb_{0.5}Gd_{0.5}Zr_2O_7$ ceramic is shown in Fig. 2. Obviously, the grain boundaries are very clean and the average grain size is several micrometers for $SmYb_{0.5}Gd_{0.5}Zr_2O_7$ ceramic.

Fig. 3 shows typical impedance spectra of $SmYb_{0.5}Gd_{0.5}Zr_2O_7$ ceramic measured at 723 K in air. The impedance spectra of $SmYb_{0.5}Gd_{0.5}Zr_2O_7$ ceramic are normally composed of a high-frequency arc and a low-frequency arc, as shown in Fig. 3. In the ideal case, the frequency response of electrical conductivity of polycrystalline electrolytes can be modeled by a resistor–capacitor (RC) pair in parallel. However, in the present case, in place of capacitor a constant phase element (CPE) is required to model the experimental data [25], as shown in Fig. 3. From fitted results, the capacitance values found for the high- and low-frequency arcs are 1.39×10^{-10} and 2.97×10^{-7} F cm^{-1} for $SmYb_{0.5}Gd_{0.5}Zr_2O_7$

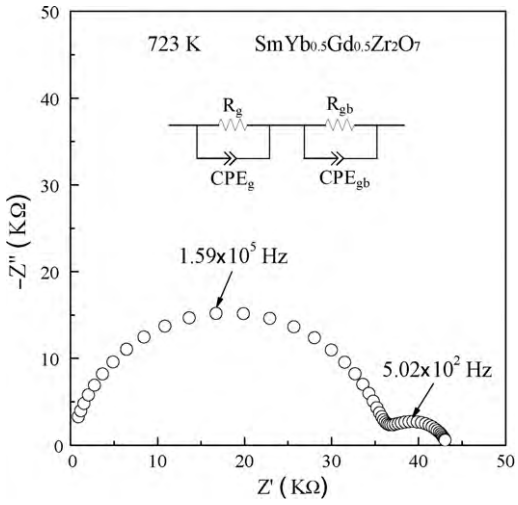

Fig. 3. Typical complex impedance and schematic equivalent electrical circuits plots for $SmYb_{0.5}Gd_{0.5}Zr_2O_7$ ceramic at 723 K. R_g, R_{gb}, CPE_g and CPE_{gb} represent grain resistance, grain boundary resistance, constant phase element of the grain and constant phase element of the grain boundary.

ceramic, which correspond to the grain and grain boundary contributions, respectively. The grain resistance value of each composition, R, is determined from the intercept of the corresponding high frequency-range semicircle on the Z' axe [26]. The grain conductivities of $SmYb_{1-x}Gd_xZr_2O_7$ ceramics are calculated from the values of resistance at corresponding temperatures and the geometrical dimensions of the measured specimens.

The temperature dependence of grain conductivity could be plotted based on the Arrhenius equation with the following expression:

$$\sigma \cdot T = \sigma_0 \ \exp\left(\frac{-E}{k_B T}\right) \quad (2)$$

where σ, T, σ_0, E and k_B are grain conductivity, absolute temperature, pre-exponential constant, activation energy and Boltzman constant, respectively. Fig. 4 shows Arrhenius plots derived from the impedance spectra over the temperature range of 723–1173 K. It can be seen that the grain conductivity data follow the Arrhenius behavior with typical correlation coefficients for linear least squares fit between 0.9997 and 0.9999, which confirms that the ionic diffusion process is thermally activated. The activation energy (E) and pre-exponential factor (σ_0) of each composition are calculated from the slope and the intercept of the linear fits in the

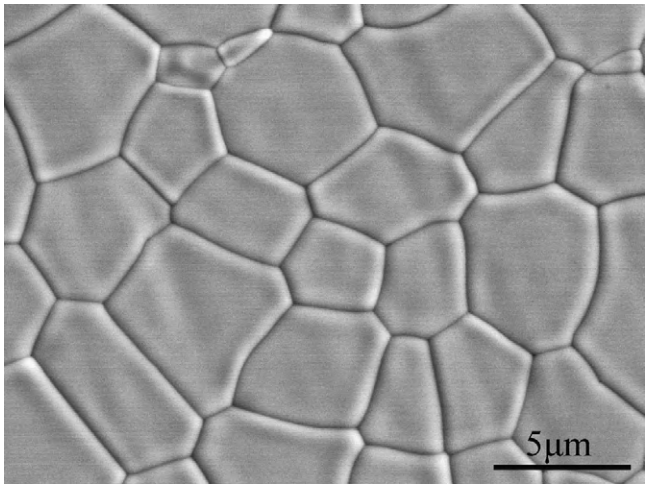

Fig. 2. Micrograph of the thermally etched surface of $SmYb_{0.5}Gd_{0.5}Zr_2O_7$ ceramic.

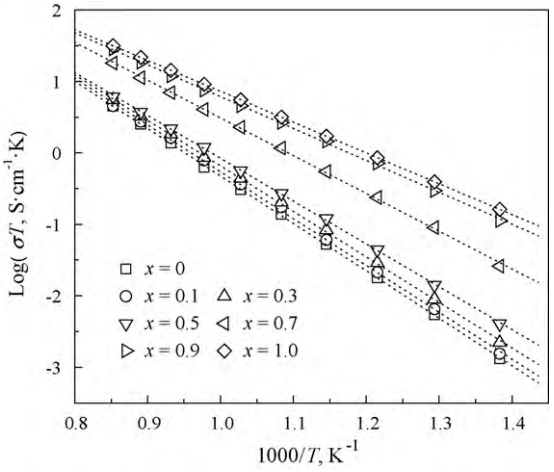

Fig. 4. Arrhenius plots of grain conductivities of $SmYb_{1-x}Gd_xZr_2O_7$ ceramics.

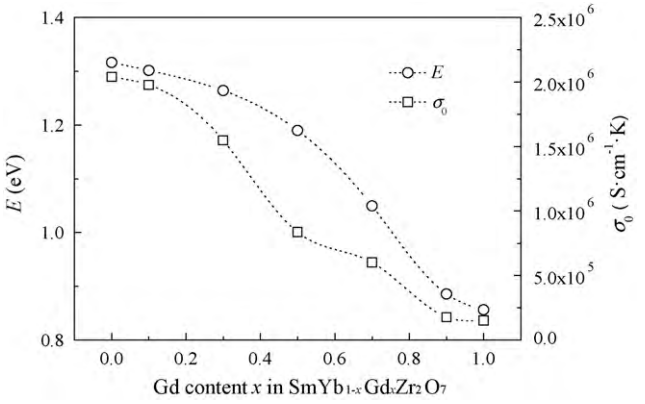

Fig. 5. Activation energy and pre-exponential factor for the grain conductivity of $SmYb_{1-x}Gd_xZr_2O_7$ ceramics.

Arrhenius plots (Fig. 4), respectively. The latter is indicative of the number of charge carriers available for conduction. The calculated values of activation energy and pre-exponential factor are presented in Fig. 5.

Fig. 6 shows the variations in grain conductivity of $SmYb_{1-x}Gd_xZr_2O_7$ ceramics as a function of gadolinium content at different temperatures. Clearly, the grain conductivity of each composition gradually increases with increasing temperature from 723 to 1173 K. The grain conductivity slightly increases with increasing gadolinium content from $x = 0$ to 0.5 at all temperature levels; however, an increase of about one order of magnitude in grain conductivity is found at all temperature levels when the gadolinium content increases from $x = 0.5$ to 0.7. With further increasing gadolinium content from $x = 0.7$ to 1.0, the grain conductivity slightly increases, and reaches a maximum value at $x = 1.0$ for all temperature levels. The highest grain conductivity value obtained in $SmYb_{1-x}Gd_xZr_2O_7$ ceramics is 2.69×10^{-2} S cm^{-1} at 1173 K for $SmGdZr_2O_7$ ceramic. From Fig. 6, the measured grain conductivity values of pyrochlore-type materials are apparently higher than those of defect fluorite-type materials in the temperature range of 673–1173 K in $SmYb_{1-x}Gd_xZr_2O_7$ ceramics. The decrease in σ_0 would lead to a decrease in electrical conductivity; however, the decrease in E would promote the oxide-ion migration. Thus, these two processes are competing. Both σ_0 and E decrease with increasing gadolinium content, as shown in Fig. 5; however, the grain conductivities always increase with increasing gadolinium content, which indicates that the decrease in σ_0 is not

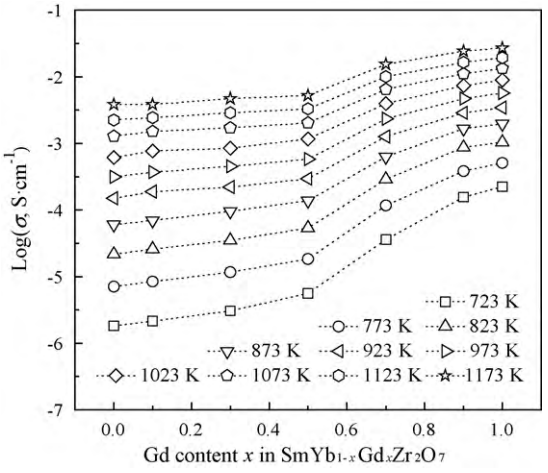

Fig. 6. Variations in grain conductivity of $SmYb_{1-x}Gd_xZr_2O_7$ ceramics as a function of gadolinium content at different temperatures.

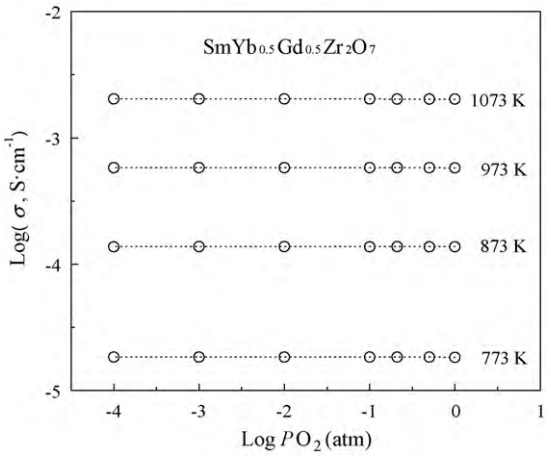

Fig. 7. Oxygen partial pressure dependence of grain conductivity of $SmYb_{0.5}Gd_{0.5}Zr_2O_7$ ceramic at different temperatures.

able to compensate for the decrease in E, and consequently causes the increase in grain conductivity.

The oxygen partial pressure $p(O_2)$ dependence of electrical conductivity was measured for $SmYb_{1-x}Gd_xZr_2O_7$ ceramics. Fig. 7 shows the grain conductivity of $SmYb_{0.5}Gd_{0.5}Zr_2O_7$ ceramic as a function of oxygen partial pressure $p(O_2)$ at different temperatures. It is evident that grain conductivity of $SmYb_{0.5}Gd_{0.5}Zr_2O_7$ is almost independent of oxygen partial pressure from 1.0×10^{-4} to 1.0 atm at all test temperature levels, which indicates that the conduction is purely oxide-ion conductive with negligible electronic conduction [27]. The results obtained in this work show that $SmYb_{1-x}Gd_xZr_2O_7$ ceramics are oxide-ion conductors from the low oxygen partial pressure to high oxygen pressure with the highest grain conductivity of 2.69×10^{-2} S cm^{-1} at 1173 K. The oxide-ion conductivities of conventional solid electrolytes such as $Zr_{0.92}Y_{0.08}O_{2-\delta}$, $Ce_{0.8}Gd_{0.2}O_{2-\delta}$, and $La_{0.80}Sr_{0.20}Ga_{0.76}Mg_{0.19}Co_{0.05}Y_{0.08}O_{3-\delta}$, which are used in SOFCs, are 9.29×10^{-2}, 1.55×10^{-1} and 2.74×10^{-1} S cm^{-1} at 1173 K [28], respectively. Taking into account that the oxide-ion conductivity of $SmYb_{1-x}Gd_xZr_2O_7$ ceramics (2.69×10^{-2} S cm^{-1} at 1173 K) is slightly lower than those of conventional solid electrolytes, the most likely applications of $SmYb_{1-x}Gd_xZr_2O_7$ ceramics in solid oxide fuel cells are high-temperature solid electrolytes, or thick-film electrolytes, or as protective layers applied onto CeO_2- or $LaGaO_3$-based solid electrolyte materials [28].

4. Conclusions

$SmYb_{1-x}Gd_xZr_2O_7$ ($0 \le x \le 0.5$) ceramics exhibit a defect fluorite-type structure, while $SmYb_{1-x}Gd_xZr_2O_7$ ($0.7 \le x \le 1.0$) ceramics have a pyrochlore-type structure. The relative densities of $SmYb_{1-x}Gd_xZr_2O_7$ ceramics pressureless-sintered at 1973 K for 10 h are higher than 96%. $SmYb_{1-x}Gd_xZr_2O_7$ ceramics are oxide-ion conductors in oxygen partial pressure range of 1.0×10^{-4} to 1.0 atm at all test temperature levels. The grain conductivity of each composition in $SmYb_{1-x}Gd_xZr_2O_7$ ceramics increases with increasing temperature from 723 to 1173 K. The grain conductivities of $SmYb_{1-x}Gd_xZr_2O_7$ ceramics gradually increase with increasing gadolinium content at identical temperature levels. An increase of about one order of magnitude in grain conductivity is found at all temperature levels when the gadolinium content increases from 0.5 to 0.7. The grain conductivities obtained in $SmYb_{1-x}Gd_xZr_2O_7$ ceramics reach the highest value of 2.69×10^{-2} S cm^{-1} at 1173 K for $SmGdZr_2O_7$ ceramic.

Acknowledgement

The authors would like to thank the financial support from the National Natural Science Foundation of China (NSFC-No. 50972030).

References

[1] H. Lehmann, D. Pitzer, G. Pracht, R. Vassen, D. Stőver, J. Am. Ceram. Soc. 86 (2003) 1338–1344.
[2] C.G. Levi, Curr. Opin. Solid State Mater. Sci. 8 (2004) 77–91.
[3] X.Q. Cao, R. Vassen, D. Stőver, J. Eur. Ceram. Soc. 24 (2004) 1–10.
[4] Z.-G. Liu, J.-H. Ouyang, Y. Zhou, J. Li, X.-L. Xia, Int. J. Appl. Ceram. Technol. 6 (2009) 485–491.
[5] J. Cheng, J.J. Li, C.Y. Ma, Z.P. Hao, Catal. Commun. 10 (2009) 1170–1173.
[6] P. Xu, K. Holliday, K.R. Czerwinski, J.C. Nino, J. Nucl. Mater. 394 (2009) 39–45.
[7] M.A. Subramanian, G. Aravamudan, G.V. Subba Rao, Prog. Solid State Chem. 15 (1983) 55–143.
[8] J.C. Boivin, G. Mairesse, Chem. Mater. 10 (1998) 2870–2888.
[9] S.J. Litzelman, J.L. Hertz, W. Jung, H.L. Tuller, Fuel Cells 8 (2008) 294–302.
[10] D.J.L. Brett, A. Atkinson, N.P. Brandon, S.J. Skinner, Chem. Soc. Rev. 37 (2008) 1568–1578.
[11] K. Shinozaki, M. Miyauchi, K. Kuroda, O. Sakurai, N. Mizutani, M. Kato, J. Am. Ceram. Soc. 62 (1979) 538–539.
[12] O. Yamamoto, Electrochim. Acta 45 (2000) 2423–2435.
[13] J.W. Fergus, J. Power Sources 162 (2006) 30–40.
[14] S. Hui, J. Roller, S. Yick, X. Zhang, C. Decès-Petit, Y. Xie, R. Maric, D. Ghosh, J. Power Sources 172 (2007) 493–502.
[15] B.P. Mandal, S.K. Deshpande, A.K. Tyagi, J. Mater. Res. 23 (2008) 911–916.
[16] Z.-G. Liu, J.-H. Ouyang, Y. Zhou, X.-L. Xia, J. Power Sources 185 (2008) 876–880.
[17] J.A. Díaz-Guillén, M.R. Díaz-Guillén, K.P. Padmasree, A.F. Fuentes, J. Santamaría, C. León, Solid State Ionics 179 (2008) 2160–2164.
[18] J.A. Díaz-Guillén, A.F. Fuentes, M.R. Díaz-Guillén, J.M. Almanza, J. Santamaría, C. León, J. Power Sources 186 (2009) 349–352.
[19] Z.-G. Liu, J.-H. Ouyang, Y. Zhou, X.-L. Xia, Electrochim. Acta 54 (2009) 3968–3971.
[20] X.-L. Xia, J.-H. Ouyang, Z.-G. Liu, S. Gao, S. Li, J. Electrochem. Soc. 157 (2010) B470–B476.
[21] Z.-G. Liu, J.-H. Ouyang, Y. Zhou, J. Alloys Compd. 472 (2009) 319–324.
[22] Z.-G. Liu, J.-H. Ouyang, Y. Zhou, M.-C. Meng, X.-L. Xia, Philos. Mag. 89 (2009) 553–564.
[23] G.S. Rohrer, Structure and Bonding in Crystalline Materials, Cambridge University Press, Cambridge, 2004, pp. 521–525.
[24] H. Yamamura, H. Nishino, K. Kakinuma, K. Nomura, Solid State Ionics 158 (2003) 359–365.
[25] J.R. Macdonald, W.B. Johnson, in: E. Barsoukov, J.R. Macdonald (Eds.), Impedance Spectroscopy: Theory, Experiment and Applications, 2nd ed., John Wiley & Sons, Inc., New Jersey, 2005 (Ch. 1).
[26] M.H. Abdullah, A.N. Yussof, J. Mater. Sci. 32 (1997) 5817–5823.
[27] J.B. Goodenough, Annu. Rev. Mater. Res. 33 (2003) 91–128.
[28] V.V. Kharton, F.M.B. Marques, A. Atkinson, Solid State Ionics 174 (2004) 135–149.